ΣΥΝΕΔΡΙΑ ΤΗΣ 4ΗΣ ΜΑΪΟΥ 1995

ΠΡΟΕΔΡΙΑ ΜΑΝΟΥΣΟΥ ΜΑΝΟΥΣΑΚΑ

ΜΗΧΑΝΙΚΗ. — **On a general numerical method for defining plasticity laws of anisotropic bodies**, by *Pericles S. Theocaris**, Fellow of the Academy.

ABSTRACT

A method is presented replacing anisotropic hardening plasticity by an appropriate sequence of anisotropic elasticity problems. Assuming a stepwise form of loading or unloading, we measure the instantaneous tension and compression yield stresses along the transient principal-stress directions. These parameters completely define the instantaneous state of anisotropy of the body for the corresponding loading step, by applying the theory of elliptic paraboloid failure locus (EPFS). The parameter identification problem is formulated on the consitutive expressions for this most general failure criterion and by applying convenient constraints derived from the EPFS theory, which are serving as filters throughout the whole procedure of evaluating the characteritic values of terms defining the variable components of the failure tensor polynomial, as the material is continuously loaded from the elastic to the plastic region, up to the ultimate failure load.

Accurate experimental data for the subsequent yield loci of various materials, were used as input data for applying the method developed. It was shown that, either the prediction, or the eventual correction of either extrapolated, or interpolated yield surfaces, are reasonable and concordant to experimental evidence. The method presents the further advantage of clearly indicating the parts contributed either by plasticity, or by the strength differential effect of elastically and plastically deformed materials and their evolution during the development of plastic deformation.

1. INTRODUCTION

The theoretical and experimental investigation of the elastoplastic be-

* Π. Σ. ΘΕΟΧΑΡΗ, **Γενικὴ μέθοδος προσδιορισμοῦ τῶν νόμων πλαστικότητος ἀνισοτρόπων ὑλικῶν.**

haviour of materials constitutes one of the basic concerns of materials science. Continuous efforts to bring to light the laws of deformation of the matter, started as early as the end of the last century, are still active. One can pretend that the study of multiaxial elastoplastic behaviour of engineering materials embraces one of the largest and most diversified systems of experiments. During these studies both proportional and non-proportional types of loading have been considered. The generalization of the theory of plastic potential, with associated and non-associated flow rules, their connection with thermodynamics and consideration of nonconvex yield surfaces [1-3] made clear that plasticity may be considered as a general and variable anisotropy, depending on the stress-strain history, the influence of the preloading in the yield surface and the contribution of the Bauschinger effect. All these subjects have been investigated by a large series of meticulous experiments and serious efforts have been made to adapt the plastic stress-strain relations and / or the expressions of the yield surfaces, including the anisotropy to these results [4-11]

In this paper a procedure is established according to whihc the general anisotropic hardening elastoplastic behaviour of a particular material is approximated by an equivalent fictitious anisotropic elastic material, whose mechanical properties are varying with the loading history of the body, thus adapted to the corresponding sets of values of the material under the loading conditions of each step of loading. It is therefore obvious that the method is superior than any other approximate method introduced up to now, and especially either the well-known Mrôz's method of bounding surfaces [12], or the method of nested multisurface, introduced by Dafalias and Popov [11, 13]. Indeed, although these two constitutive models describe the plastic deformation of elastoplastic bodies under any complicated loading path and for the most general material, yet the method introduced in this paper yields more accurate results, by rectifying some weaknesses of these models and, furthermore, and most important, by indicating clearly the contributions of either plasticity or the strength differential effect to the subsequent state of loading of the material.

2. FORMULATION OF THE METHOD

The present method considers a learning process for an appropriately defined numerical procedure based on the least squares method with constrained

conditions, based on the validity of the failure tensor polynomial used as a constitutive condition for progressive yielding. Then, the method consists in the construction of a numerical procedure, trained to fit existing experimental results, and to extend these results, which are normally obtained either in the tension-tension-tension octant, or the respective compression octant, of the principal stress space, to the whole stress space. Having totally defined some intermittent particular yield loci of the material, based on a sufficient number of experimental points, it is possible to combine this method with the related modern method, based on a neural network approach, which allows to determine further subsequent yield loci to the esixting already experimental yield surfaces, by considering the material as a *progressively changing anisotropic one*, whose variation of anisotropy is due to a further development of plasticity of the initial plastic enclaves [19]. The neural network is then instructed to *learn* the law of variation af anisotropy of the material, and, if applied to another set of experimental data, may fulfil its task to define the next step in shorter times and with higher accuracy. Both methods, making use of the flexibility of the failure tensor polynomial criterion, (FTP), expressed by an elliptic paraboloid failure surface (EPFS), can establish the equivalent elastic failure characteristics, by using a continuously variable form of the EPFS. The details of the theory of the methods are fully presented in refs. [14-18] and [19, 20].

In this paper we are concerned only with the numerical method based on least square theory with constraints. This method may replace the classical numerical methods for elastoplastic calculations, since it takes into account, in a more judicious manner, the experimental data, and automatically improves itself, through *learning*. The method has been applied to concrete problems, where we dispose a series of experimental data from reliable tests (uniaxial or multiaxial), and we seek to establish the failure locus of the material tested, assuming that it represents the most general of mechanical behaviour (orthotropic material) and subjected to any complicated loading path, either inside the elastic, or outside this region, where its failure locus is variable with loading.

3. DESCRIPTION OF THE METHOD

In order to establish the general failure surface of a brittle material under

the most general type of external triaxial loading and assuming that the material is in principle generally orthotropic, it is necessary to run a series of complicated triaxial tests. The main characteristics of the testing device are, therefore, a uniformly distributed and independently controlled device of application of a triaxial type of principal stresses, complemented by a system of accurate and rapidly measured strains in a large range of deformations, whereas the machine is a robust one, which disposes a high capacity of sustaining stresses of the order of 250 MPa [21].

For establishing the strength behaviour of this type of brittle rock under a triaxial mode of loading, a series of tests were conducted along loading paths following either the hydrostatic axis in the stress space, or paths with varying $\sigma_2 = \sigma_3$ stresses, while the σ_1- principal stress was kept constant, or path in which the σ_1- and σ_2-stresses are kept constant at various levels and the σ_3-stress is increased up-to-yielding and ultimate strength of the material [21]. Figures 1 to 3 present the strength data for initial yielding (Fig. 1) and for ultimate strength (Fig. 2) from the tests where the σ_1-stress was kept constant at various steps of loading, whereas, in Fig. 3, strength results are given for the case of loading, where the σ_2-stress was kept constant, whereas the σ_1- and σ_3-components of stresses varied, up to the ultimate loading. All

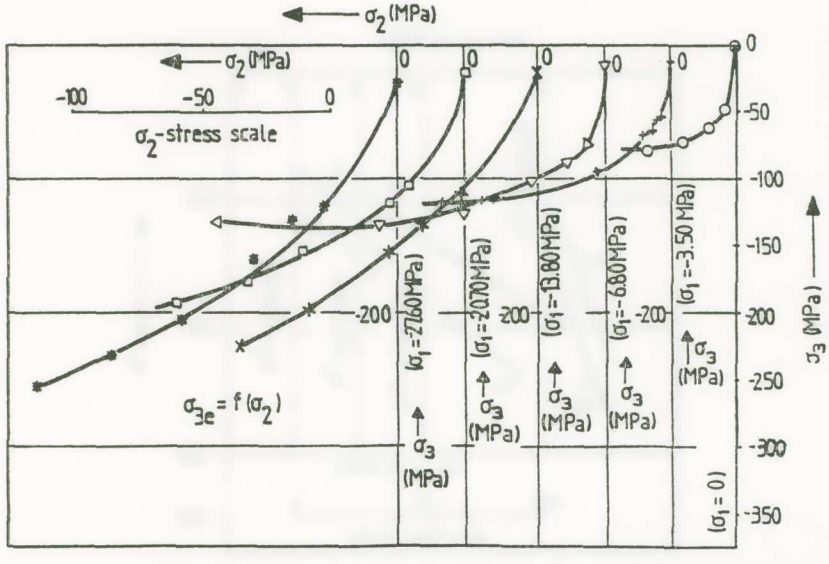

Fig. 1. Yield limits at the conventional yield point in the (σ_2, σ_3)-principal stress plane for parametric values of the σ_1-principal stress.

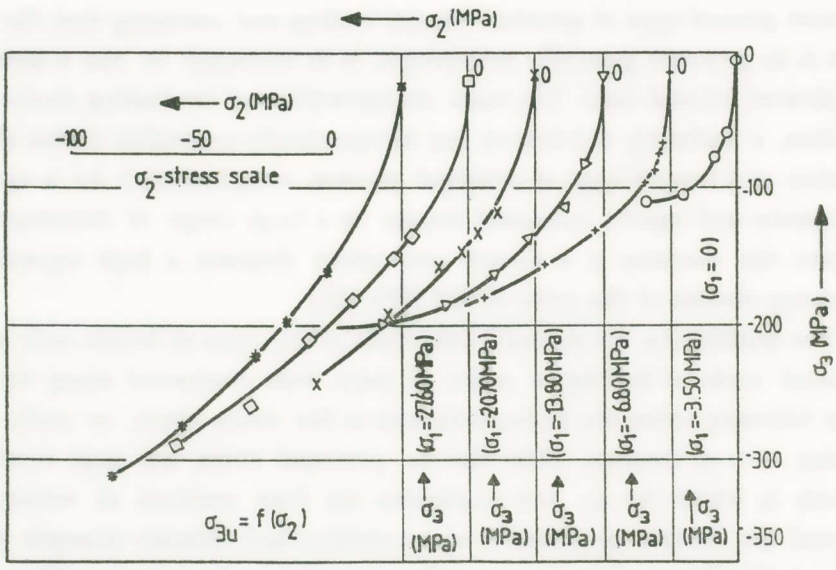

Fig. 2. Yield limits at the ultimate strength of material in the (σ_2, σ_3)-principal stress plane for plane for parametric values of the σ_1-principal stress.

these strength data will be used for establishing the failure locus of this anisotropic material, by applying the method propounded in this paper, and checking its efficiency and degree of reliability.

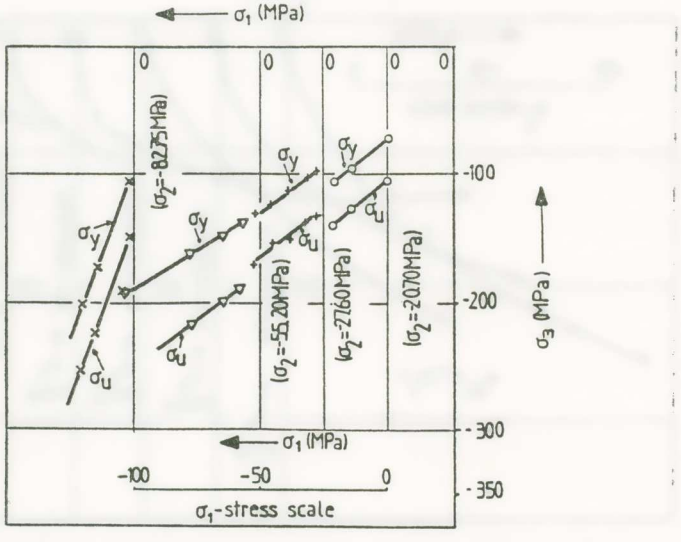

Fig. 3. Yield limits at the conventional (σ_y), and ultimate strength (σ_u), yield points in the (σ_1, σ_3)-principal stress plane for parametric values of the σ_2-principal stress.

The problem posed for the general anisotropic elastoplasticity law with respect to a given body may be expressed as follows: «Determine an anisotropic piecewise linear elasticity sequence of laws, for which a body with the same geometry, the same loading and the same constraints, exhibits a behaviour identical with the behaviour of the elastoplastic anisotropic body under study».

If the loading function p(t) of the time $t \in [0, T]$ is given, we may divide [0, T] into the time instants $t^{(1)}, t^{(2)}, \ldots, t^{(n)}$ and denote by $C^{(1)}, C^{(2)}, \ldots, C^{(n)}$ the corresponding, but as yet unknown, anisotropic elasticity tensors, satisfying the well-known symmetry and ellipticity conditions. We seek $\{t^{(\rho)}, C^{(\rho)}\}$, $\rho = 1,\ldots,n$, such that the solution of the anisotropic elasticity problem approximates as close as possible the solution of the initial anisotropic elastoplasticity problem. The problem is formulated as a parameter identification problem, where $z^{(\rho)} = \{t^{(\rho)}, C^{(\rho)}\}$ are the control parameters and the strain-, stress-, and displacement— fields are the state functions. The control parameters will be calculated by taking into account the experimental results as observation conditions. Assuming steps of small deformations, we denote by A_1, A_2 and A_3 the following differences:

$$A_1 = \sum_{\rho=1}^{n} \int_{\Omega} \left[u_{pl}^{(\rho)} - u_{el}^{(\rho)} \right]^2 d\Omega,\ A_2 = \sum_{\rho=1}^{n} \int_{\Omega} \left[\varepsilon_{pl}^{(\rho)} - \varepsilon_{el}^{(\rho)} \right]^2 d\Omega,\ A_3 = \sum_{\rho=1}^{n} \int_{\Omega} \left[\sigma_{pl}^{(\rho)} - \sigma_{el}^{(\rho)} \right]^2 d\Omega \quad (1)$$

where u, ε and σ are respectively the displacements, strains and stresses, Ω is the body under consideration and the subscripts «el» and «pl» denote elastic or plastic quantities respectively.

The problem reads: Find $z^{(\rho)} = \{t^{(\rho)}, C^{(\rho)}\}$, $\rho = 1, \ldots, n$, such as to satisfy:

$$A_1 + A_2 + A_3 \rightarrow \min \quad (2)$$

where for every ρ, the quantities $\sigma_{el}{}^{(\rho)}$, $\varepsilon_{el}{}^{(\rho)}$ and $u_{el}{}^{(\rho)}$ satisfy the equations of equilibrium, the strain-displacement relations and the material law:

$$\varepsilon_{el}^{(\rho)} = C^{(\rho)}\, \sigma_{el}^{(\rho)} \quad (3)$$

The quantities $\varepsilon_{pl}{}^{(\rho)}$, $\sigma_{pl}{}^{(\rho)}$, $u_{pl}{}^{(\rho)}$, must satisfy the equilibrium equations, the plasticity rule, and must agree with the experimental results concerning the relations between $\varepsilon_{pl}{}^{(\rho)}$ and $\sigma_{pl}{}^{(\rho)}$. Moreover, the quantities for both the initial plastic and elastic problems must satisfy the boundary conditions and the initial consitions at $t = 0$.

Even in the case of problems of elastoplasticity, where the A_1-condition, expressed by the first relation (1), may be ignored in the process and only as a checking condition of compatibility may be used, the arising parameter identification problem is of a non-classical nature and, therefore, it cannot be effectively treated by classical optimization methods. If we simplify the problem by discarding the A_1-condition and impose the discretized form of the elastic body to minimize the (A_2+A_3)-deviation, the resulting condition takes the form:

$$\sum_{\rho=1}^{n}\left[\sum_{r=1}^{m}\left(\left\|\varepsilon_{pl}^{(\rho)(r)}-\varepsilon_{el}^{(\rho)(r)}\,z^{(\rho)}\right\|^{2}+\left\|\sigma_{pl}^{(\rho)(r)}-\sigma_{el}^{(\rho)(r)}\,(z^{(\rho)})\right\|\right)\right]\to\min \tag{4}$$

$$K(z^{\rho})\;u^{(\rho)}+p^{(\rho)}=0 \tag{5}$$

where $r=1,\ldots,m$ enumerates the discrete degrees of freedom, $K(.)$ is the elasticity stiffness matrix and the symbol $\|\ .\ \|$ denotes the corresponding Euclidean norms. The stiffness matrix K corresponds to the geometry of the body, whose quantities $\sigma_{pl}^{(\rho)}$ and $\varepsilon_{pl}^{(\rho)}$ are defined experimentally at the time intervals $t^{(\rho)}$. Finally, $p^{(\rho)}$ is the loading function, which leads to the experimental results at the ρ-step.

Note that relation (4) can be replaced by [17, 18]:

$$\max_{\rho,\,r}\left\{\left\|\varepsilon_{pl}^{(\rho)(r)}-\varepsilon_{el}^{(\rho)(r)}\,z^{(\rho)}\right\|+\left\|\sigma_{dl}^{(\rho)(r)}-\sigma_{el}^{(\rho)(r)}\,z^{(\rho)}\right\|\right\}\to\min \tag{6}$$

or, by the prescribed error inequalities:

$$\max_{p.r.i.j}\left|\varepsilon_{plij}^{(\rho)(r)}-\varepsilon_{elij}^{(\rho)(r)}\,z^{(\rho)}\right|\leqslant\delta,\ \max_{p.r.i.j}\left|\sigma_{plij}^{(\rho)(r)}-\sigma_{elij}^{(\rho)(r)}\,(z^{(\rho)})\right|\leqslant\delta, \tag{7}$$

The inequalities (7) imply that the maximum differences between the elastic and the plastic stress-and strain-components respectively at any point of the body, and at any control moment $t^{(\rho)}$, cannot be larger than a given constant δ. We note further that the control instant $t^{(\rho)}$ may be replaced by a control strain, if the loading - unloading sequence is given. If the control strains are given, then $p^{(\rho)}$ results from the prescribed strains or strain-variations at the ρ-step.

For the classical experimental procedures, that is for a given sequence of

strains, even in different directions, we can assume that z includes only the anisotropic elasticity moduli $C^{(\rho)}$, where we assign at each loading step several control parameters, $C(^{\rho}_{1})$, $C(^{\rho}_{2})$, ..., $C(^{\rho}_{\nu})$, in order to approximate, in a reliable manner, the anisotropic plasticity stress - and strain - fields. In this way the parameter identification problem is an inverse problem in structural analysis, where a solution is prescribed and we ask for convenient elastic properties and / or loading and / or geometric quantities, producing a solution very close, or identical, to the prescribed one. Obviously, we have to solve a minimum deviation problem having as subsidiary conditions all the relations characterizing the solution. Indeed, in adapting the structural analysis to the numerical approximation computation, it is necessary to formulate the structural analysis problem as a minimization problem and the same procedure is used for the parameter identification problem described by relations (4) and (5), where a quadratic deviation function should minimized. Then, we have to solve the linear system (5) corresponding to a linear elastic structure for each value of the control vector $z^{(\rho)}$.

If now the components of strains and stresses, $\varepsilon_{el}{}^{(\rho)}$ and $\sigma_{el}{}^{(\rho)}$, corresponding to the displacements $u_{el}{}^{(\rho)}$, are prescribed, or they must take values very close to respective $\varepsilon_{pl}{}^{(\rho)}$ -, $\sigma_{pl}{}^{(\rho)}$ -values, for all stresses and strains of the structure under consideration, and for all ρ, we need to determine the control vectors $z^{(\rho)}$, $\rho = 1, ..., n$, i.e. to the corresponding control times $t^{(\rho)}$, as well as the elasticity coefficients $C^{(\rho)}$, such as to minimize the differences in (4) after an appropriate discretization of the structure. For each value of $z^{(\rho)}$, $\rho = 1,...,n$, the structure will be calculated by means of the numerical procedure, introduced through Eqs. (6) and (7).

4. A GENERAL FAILURE CRITERION EXPRESSED BY TENSOR POLYNOMIALS

A generalization of failure for *orthotropic solids* is expressed by means of the geometric interpretation of the failure surface in the principal stress space. It was shown [18] that the failure surface for orthotropic materials is an *elliptic paraboloid* with a symmetry axis parallel to the hydrostatic axis and displaced from the origin of the coordinate system by an amount depending on the degree of strength anisotropy of the material. The failure condition expressed in terms of principal stress components, σ_i, was shown to have the general form of the quadric surface equation, expressed by:

$$f(\boldsymbol{\sigma}) = \boldsymbol{\sigma} \cdot \mathbf{H} \cdot \boldsymbol{\sigma} + \mathbf{h} \cdot \boldsymbol{\sigma} - 1 = 0 \qquad (8)$$

where **H** and **h** denote 4th and 2nd-rank *failure tensors* respectively.

The tensorial character of function $f(\boldsymbol{\sigma})$ implies the *form-invariancy*, of eq. (8) and it is holding for any coordinate system transformation. Besides, the linear polynomial term, $\mathbf{h}.\boldsymbol{\sigma}$, accounts for the strength differential effect and thus, eq. (8), after a proper determination of failure tensors **H** and **h**, may constitute a valid generalization of the paraboloidal failure surface criterion for anisotropic solids. Symmetry properties of tensor **H** follow those of elastic compliance 4th-rank tensor **S**. The 2nd-rank failure tensor, **h**, may have, in general, six independent components, whereas, for specially orthotropic media, or of increased symmetry, tensor **h** becomes *axisymmetric* degenenerating to a *spherical tensor* for the isotropic medium.

The necessary and sufficient condition for the failure hypersurface of eq. (8) to be convex and open-ended is that tensor **H** must be positive semi-infinite, which means that [14]:

$$\boldsymbol{\sigma} \cdot \mathbf{H} \cdot \boldsymbol{\sigma} \geqslant 0, \qquad (\forall\, \boldsymbol{\sigma} > 0) \qquad (9)$$

Then, a necessary condition to be satisfied by the contracted components of the 4th-rank tensor **H** is given by:

$$H_{ii}\, H_{jj} - H_{ij}^2 \geqslant 0 \qquad (i,j = 1,\ldots,6) \qquad (10)$$

The convexity of the failure hypersurface, together with its open end along a triaxial path of normal stresses, postulates which are assured by the validity of either inequality (9), or (10), constitute the basic constraint implied for the validity of the least square numerical approximation in expressing the respective failure hypersurface.

The normal components of the failure tensors are expressed by:

$$H_{ii} = 1/\sigma_{Ti}\sigma_{Ci} \qquad (i \leqslant 3) \qquad (11)$$

$$h_i = (1/\sigma_{Ti}) - (1/\sigma_{Ci}) = (\sigma_{Ci} - \sigma_{Ti})H_{ii} \qquad (12)$$

whereas shear components are given by:

$$\begin{aligned} H_{ii} &= 1/\sigma_{si}^{+}\sigma_{si}^{-} \qquad (i > 3) \\ h_i &= (1/\sigma_{si}^{+}) - (1/\sigma_{si}^{-}) = (\sigma_{si}^{-} - \sigma_{si}^{+})H_{ii} \end{aligned} \qquad (13)$$

In the above relations the repeated index convention does not apply and the σ_{Ti} and σ_{Ci} - stresses express the tension (T) and compression (C) failure stresses in the i-direction. Furthermore, the σ_{si}^{+}, σ_{si}^{-}-stresses express the shear strengths, positive or negative, in the i-plane ($i > 3$) and the usual contracted notation of Cartesian indices is used, meaning, that index 4 corresponds to natural indices 23, index 5 to 13 and index 6 to 12. For the ortgotropic materials, when the coordinate system, defining the failure stresses, coincides with the material symmetry directions, there is no shear-strength differential effect, that is: $\sigma_{si}^{+} = \sigma_{si}^{-}$.

Up to this point, the failure tensor components given in relations (11) to (13) may be determined without recourse to a special phenomenological hypothesis. The evaluation of these components is based upon standard basic requirements, common for all anisotropic failure criteria, which can be expressed by the general form of eq.(8). This leaves the off-diagonal components of the failure tensor **H** (H_{ij}, $i \neq j$) to be derived according to the particular assumptions, which are different for the various criteria.

The open end of the failure hypersurface is mathematically assured by imposing the 4th-rank failure tensor **H** to have a *zero eigenvalue*. Moreover, the hypothesis that hydrostatic stress is a safe loading path is further formulated mathematically by associating the zero eigenvalue of tensor **H** to the 2nd -rank spherical tensor, **1**, which is then an *eigentensor* of **H**. The following relation holds:

$$\mathbf{H} \cdot \mathbf{1} = 0 \tag{14}$$

Among the six equations contained in relation (14) the following three relations interrelate the off-diagonal terms of the **H**-tensor with the respective diagonal ones. These equations are given by:

$$H_{ij} = 1/2\,(H_{kk} - H_{ii} - H_{jj}),\ (i, j, k \leq 3,\ i \neq j \neq k) \tag{15}$$

Relations (15) imply that the interaction failure coefficients H_{12}, H_{23} and H_{31} of the elliptic paraboloid failure surface (EPFS) are interrelated with the diagonal components, which are directly defined through relations (11) and (12) with the basic strength data. This is a significant advantage of the EPFS-criterion, which is not met with other similar criteria.

For the complete study of the elliptic paraboloid surface four types of interections are deesmed as necessary. These intersections are:

i) The principal diagonal intersections defined by planes containing one principal stress axis and the bisector of the right angle formed by the remaining principal axes.

ii) The deviatoric π-plane, which is normal to the hydrostatic axis.

iii) The principal stress plane intersections, which are convenient for the study of the mechanical properties of the anisotropic body when thin plates of the material under plane-stress conditions are to be studied.

iv) The intersections of the EPFS-surface by planes defined by the axis of symmetry of the paraboloid and either principal axis of the elliptic intersection by the deviatoric plane.

The elliptic paraboloid failure surface for the general orthotropic material is expressed, in the $(\sigma_1,\sigma_2,\sigma_3)$-principal stress space, by a complete polynomial of the second degree [14]:

$$H_{11}\,\sigma_{12} + H_{22}\,\sigma_{22} + H_{33}\,\sigma_{32} + (H_{33} - H_{11} - H_{22})\,\sigma_1\,\sigma_2 + (H_{11} - H_{22} - H_{33})\,\sigma_2\,\sigma_3 + (H_{22} - H_{33} - H_{11})\,\sigma_1\,\sigma_3 + h_1\,\sigma_1 + h_2\,\sigma_2 + h_3\,\sigma_3 = 1 \qquad (16)$$

This second-degree polynomial, referred to the Cartesian coordinate system Oxyz, where the Oz-axis is parallel to the hydrostatic axis and the (Oxy)-plane coincides with the deviatoric plane with the Oy-axis lying on the $(\sigma_3\delta_{12})$-principal diagonal plane, (δ_{12} being the bisector of the $\sigma_1\,0\sigma_2$-angle) is expressed by (see Fig. 4):

$$(H_{11} + H_{22} - 1/2\,H_{33})\,x^2 + 3/2\,H_{33}\,y^2 + \sqrt{3}(H_{11} - H_{22})\,xy + 1/\sqrt{2}\,(h_2 - h_1)\,x + 1/\sqrt{6}\,(2h_3 - h_1h_2)\,y + 1/\sqrt{3}\,(h_1 + h_2 + h_3)\,z = 1 \qquad (17)$$

Figure 4 presents the mapping of the paraboloid in the principal stress space $(0\sigma_1\sigma_2\sigma_3)$, as well as the new Cartesian coordinate systems (Oxyz) and (0''x''y''z'') corresponding to the already defined system and the Cartesian system whose 0''z''-axis is parallel to the hydrostatic axis (Oxy), whereas the O''x'' - and O''y'' axes lie again on the deviatoric plane but they are created by an angular displacement on the (Oxy)-system so that the new (O''x''y'')-system coincides with the principal axes of the elliptic intersection of the EPFS by the deviatoric plane. Then, the deviatoric plane is defined at once by putting in relation (17) the value $z = 0$.

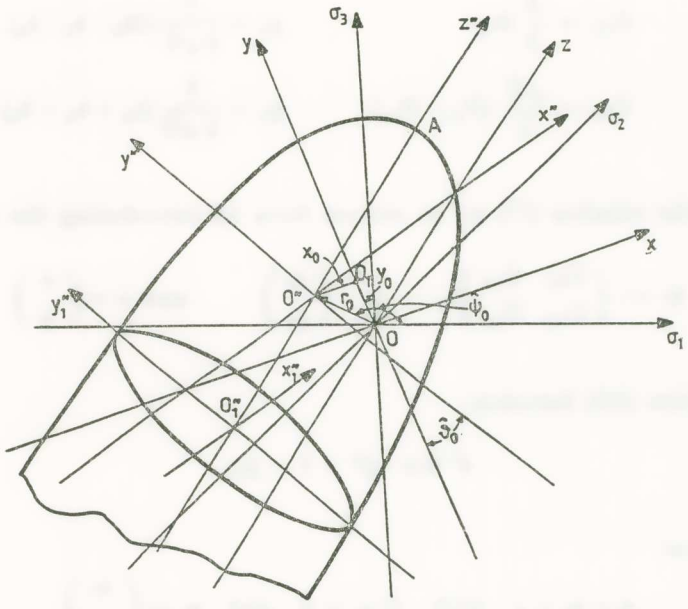

Fig. 4. The elliptic paraboloid failure surface (EPFS) for the general orthotropic material.

The principal diagonal intersection of the elliptic paraboloid failure surface by the plane (σ_3, δ_{12}), where σ_3 is the strong principal stress axis and δ_{12} is the bisector of the angle $\sigma_1 O \sigma_2$, is defined as follows. For the general orthotropic body the equation of the intersection of the failure locus and the (σ_3, δ_{12})-plane is given by:

$$1/2\,(H_{11} + H_{22} + 2H_{12})\,\delta_{12}^2 + H_{33}\,\sigma_3^2 + \sqrt{2}\,(H_{13} + H_{23})\,\delta_{12}\,\sigma_3 + \\ + \sqrt{2}/2\,(h_1 + h_2)\,\delta_{12} + h_3\,\sigma_3 - 1 = 0 \qquad (18)$$

The other two principal diagonal intersection of the EPFS-surface by the planes (σ_1,δ_{23}) and (σ_2,δ_{13}) can be readily established from relation (18) by cyclic interchange of the respective indices.

Relation (17) in the Oxyz-space may be written as follows:

$$G_{xx}\,x^2 + G_{yy}\,y^2 + 2\,G_{xy}\,xy + 2\,g_x + 2\,g_x\,y + g_z\,z = 1 \qquad (19)$$

where:

$$G_{xx} = \left(H_{11} + H_{22} - \frac{1}{2}\,H_{33}\right) \quad g_x = \frac{1}{2\sqrt{2}}\,(h_2 - h_1)$$

$$G_{yy} = \frac{3}{2} H_{33} \qquad g_y = \frac{1}{2\sqrt{6}} (2h_3 - h_1 - h_2) \tag{20}$$

$$G_{xy} = \frac{\sqrt{3}}{2} (H_{11} - H_{22}) \qquad g_x = \frac{1}{2\sqrt{3}} (h_1 + h_2 + h_3)$$

We refer relation (17) to its normal form by introducing the relations:

$$\mathbf{G} = - \begin{pmatrix} G_{xx} & G_{xy} \\ G_{xx} & G_{xy} \end{pmatrix}, \quad \mathbf{g} = \begin{pmatrix} g_y \\ g_x \end{pmatrix} \quad \text{and} \quad z = \begin{pmatrix} x \\ y \end{pmatrix} \tag{21}$$

Then, relation (19) becomes:

$$\mathbf{z}^T \mathbf{G}\, \mathbf{z} - \mathbf{g}^T + 1 = g_z z \tag{22}$$

Putting now:

$$\mathbf{z} = \mathbf{z}_c + r \quad \text{with} \quad \mathbf{G}\, \mathbf{z}_c = g \quad \text{and} \quad \mathbf{z}_c = \begin{pmatrix} x_c \\ y_c \end{pmatrix} \tag{23}$$

and introducing these relations into Eq. (22), we obtain:

$$g_z z = 1 - \mathbf{g}^T \mathbf{z}_c + \mathbf{r}^T \mathbf{G}\, \mathbf{r} \tag{24}$$

Putting:

$$z = z_e + \Delta z \quad \text{with} \quad g_c z_c = 1 - \mathbf{g}^T \mathbf{z}_T \tag{25}$$

into relation (24), we readily derive that:

$$g_z \Delta z = \mathbf{r}^T\, \mathbf{G}\mathbf{r} \tag{26}$$

where x_c and y_c are the coordinates of the center of the curves representing the intersection of the failure hypersurface by any plane and z_c is the distance of this center from the origin. Then, it is valid that:

$$\begin{aligned} G_{xx} x_c + G_{xy} y_c &= - g_x \\ G_{xy} x_c + G_{yy} y_c &= - g_y \\ g_z z_c &= 1 + (g_x x_c + g_y y_c) \end{aligned} \tag{27}$$

From relations (23, 1 and 3) it becomes evident that:

$$\mathbf{r} = \begin{pmatrix} \Delta x \\ \Delta y \end{pmatrix} \text{ and therefore } \begin{matrix} x = x_c + \Delta x \\ y = y_c + \Delta y \\ z = z_c + \Delta z \end{matrix} \tag{28}$$

Equation (26), through an analysis for eigenvalues of **G**, yields:

$$\mathbf{G} = \mathbf{C}\,\mathbf{D}\,\mathbf{C}^T \tag{29}$$

$$\mathbf{D} = \begin{pmatrix} d_1 & 0 \\ 0 & d_1 \end{pmatrix} \text{ and } \mathbf{C} = \begin{pmatrix} c_{x_1} & c_{x_2} \\ c_{y_1} & c_{y_2} \end{pmatrix} \tag{30}$$

where d_1, d_2 are the respective eigenvalues of **G**. Similarly, the angular displacement of the axes of the intersection studied is given by the eigenvectors:

$$\mathbf{s} = \mathbf{C}^T\mathbf{r} \quad \text{and} \quad \mathbf{r} = \mathbf{C}\,\mathbf{s} \tag{31}$$

Introducing these values into relation (26) we derive the equation:

$$g\Delta z = d_1 s_1^2 + d_2 s_2^2 \tag{32}$$

If the eigenvalue d_2 is larger than d_1 and both eigenvalues are positive, the lengths of the principal axes of the intersection under study are given by:

$$a_1 = \left(\frac{g_z \Delta z}{d_1} \right)^{1/2} \text{ and } \quad a_2 = \left(\frac{g_z \Delta z}{d_2} \right)^{1/2} \tag{33}$$

For these lengths the a_1-axis is the longer and a_2 is the shorter for $d_2 > d_1 > 0$. Then, the expression for the curve representing the intersection of the hypersurface can be readily found to be:

$$\left(\frac{s_1}{a_1} \right)^2 + \left(\frac{s_2}{a_2} \right)^2 = 1 \tag{34}$$

For $z = 0$, from which we derive the intersection of the elliptic paraboloid by the π-deviatoric plane, we have $\Delta z = -z_c$ and

$$\begin{aligned} s_1 &= a_1 \cos\theta \\ s_2 &= a_2 \sin\theta \end{aligned} \tag{35}$$

When the eigenvalues d_i present the sequence $d_1 > 0 > d_2$ we obtain an hyperbolic intersection, which must be rejected [22, 23].

This condensed theory, concerning the definition of the form and dimensions of the curves derived by the intersections of the elliptic paraboloid failure surface, replace the analytic expressions of the forms of various intersections of the failure surface given in refs. [15-18].

5. NUMERICAL APPLICATIONS

The approximation schemes developed in the previoussections will now be applied for the treatment of a numerical application. We consider the experiments described in section 3 of this paper, concerning the failure modes of a coarse grained dense crystalline material, whose strength differential effect is predominant in its mode of failure. It is assumed that the stress data given in Tables 1 and 2 are the data for the parameter identification problem of the

TABLE 1

The values of the terms of the elliptic paraboloid failure surface, as well as the characteristic quantities defining the deviatoric and the principal (σ_3, δ_{12}) diagonal plane intersections of the EPFSs.

Loading Steps	H_{11}	H_{22}	H_{33}	h_1	h_2	h_3	Remarks
Elastic (I)	0.19380	0.63794	0.21215	36.0586	0.12897	0.19375	All H &
Initial Yielding (II)	0.16969	0.42635	0.09545	27.743	0.11351	0.15328	h must be
Ultimate Strength (III)	0.34174	0.85537	0.15794	60.919	0.13114	0.14247	multiplied by ($\times 10^{-3}$)

Deviatoric Plane

	x_0	y_0	s_0	ψ_0	$\alpha^1/2$	$\alpha^2/2$	θ_0
Elastic (I)	-82.59	-122.79	-147.98	-56.08°	184.36	55.48	-58.95°
Initial Yielding (II)	-91.01	-180.56	-202.20	-63.25°	254.01	67.03	-66.17°
Ultimate Strength (III)	-158.24	-349.46	-383.62	-65.64°	412.14	61.86	-67.36°

(σ_3, δ_{12})-diagonal plane ($s = \alpha y^2 + \beta y + \gamma$)

	α	β	γ	δ_{12p}	σ_{3p}	η^3	ξ^3
Elastic (I)	0.01515	-0.69581	-47.609	32.138	50.850	22.97	17.51
Initial Yielding (II)	0.008854	-0.6955	-61.8383	38.966	75.656	39.27	17.82
Ultimate Strength (III)	0.006706	-0.70217	-28.3047	7.892	69.702	52.37	19.22

form (4) and (5), with the slight modification, that, in (4), only the stress difference terms exist and the strains are not taken into account. Moreover, we have followed the loading - unloading procedures, as described in the experiments of section 3 and we have assumed as unknowns of the problem only the two-dimensional anisotropic elasticity coefficients. Thus, we can approximate the anisotropic hardening plasticity behaviour, including the strength differential (the Bauschinger) effect with a variable linear elastic behaviour defined by the appropriate changing anisotropy.

The aim of the present numerical application is the following:

i) We consider as given the experimental yield points on the failure surfaces for subsequent loading steps inside the elastic-plastic region of loading and unloading of the specimens. On each given yield surface we take a finite number of points $\sigma_{ij} = (i=j=1,2,3)$ and we apply with respect to all given yield surfaces the numerical procedure of the previous section. We assume that the elastic material is orthotropic, of changing anisotropy with loading, and we want to determine the sequence of the orthotropy coefficients $\alpha_{11}^{(\rho)}$, $\alpha_{22}^{(\rho)}$, $\alpha_{12}^{(\rho)} = a_{21}^{(\rho)}$, $\alpha_{33}^{(\rho)}$ within each element, which satisfy the identification problem for the stresses and constitute the elasticity tensor $C^{(\rho)}$ at the ρ-step of the learning algorithm. As $\rho \to \infty$ we have theoretically the solution tensor $C = \{\alpha_{11}, \alpha_{22}, \alpha_{12} = \alpha_{21}, \alpha_{33}\}$. We recall here that $\varepsilon_x = \alpha_{11}\sigma_x h + \alpha_{12}\sigma_y h, \ldots, \gamma_{xy} = \alpha_{33}\sigma_{xy} h$, where $h = 1$ mm is the thickness of the plane structure. The yield point is defined by the limit stress, which corresponds to a plastic strain of 0.02 percent [7].

ii) In order to get a more reliable approximation of the anisotropic elastoplastic problem with a sequence of anisotropic elastic problems, we have considered intermediate yield points through interpolation between two experimentally given failures in the 3D-stress space. The interpolation is guided by assuming that the stress point lies on the elliptic paraboloid failure surface, for the general anisotropic hardening elastoplastic body presenting the strength differential effect [16-18]. The failure surface in any principal stress plane is an ellipse, which can be defined from a series of points. The same property is valid for the deviatoric plane, as well as for any intersection parallel to this plane. The only exception to the general rule holding for the (EPFS)-criterion is for intersections of the failure paraboloid by planes containing the hydrostatic axis or the axis or symmetry of the paraboloid. These intersections are all parabolas [17, 18].

After the initial rough guess of a family of yield surfaces from a series of different experimentally determined triads of values of the principal stresses leading to different points of presumably the same yield surface, we obtain a family of slightly different failure loci corresponding to equivalent loading steps, but of different loading paths in the three dimensional principal stress space.

In this way three different loading steps were studied and plotted in this paper, that is the initial yield surface of impending plasticity, where the elastic version of the EPFS criterion is valid, the conventional yield surface cor-

TABLE 2

The values of the characteristic quantities defining the (σ_1, σ_2), (σ_1, σ_3), and (σ_2, σ_3) principal stress intersections for the EPFSs.

Principal Stress Plane (σ_1, σ_2)(*)

Loading Steps	σ_{M1}	σ_{2M}	λ_{12}(**)	r_{12}	α_{2M}	α_{1M}	θ_{12}(**)
Elastic (I)	-416.54	-202.38	-25.91°	463.10	154.09	202.38	-27.18°
Initial Yielding (II)	-611.12	-358.90	-30.42°	708.72	128.04	753.11	-31.43°
Ultimate Strength (III)	-1167.38	-709.18	-31.28°	1365.91	176.27	1389.72	-31.85°

Principal Stress Plane (σ_1, σ_3)(*)

	σ_{1M}	σ_{3M}	λ_{23}(**)	r_{13}	α_{1M}	α_{3M}	θ_{13}(**)
Elastic (I)	-74.93	-137.87	-47.26°	156.92	184.36	55.48	-42.74°
Initial Yielding (II)	-135.85	-113.92	-39.98°	-177.30	256.14	114.00	-57.36°
Ultimate Strength (III)	-241.31	-214.71	-24.36°	-323.00	412.14	81.86	-58.66°

Principal stress plane (σ_3, σ_2)(*)

	σ_{2M}	σ_{3M}	λ_{23}(**)	r_{23}	α_{2M}	α_{3M}	θ_{23}(**)
Elastic (I)	-1.64	-3.00	-61.27°	-3.42	171.81	35.01	-61.49°
Initial Yielding (II)	-1.95	-4.40	-66.10°	4.81	227.65	44.62	-66.61°
Ultimate Strength (III)	-1.53	-3.71	-67.55°	-4.02	210.59	31.78	-68.04°

* All stresses in MPas.

** Negative angles are measured from the negative principal axes with the lower index.

responding to an equivalent strain e = 0.002, and finally the ultimate strength failure locus corresponding to the maximum effective stress σ_u. For the evaluation of the corresponding EPFS's the respective values for σ_1, σ_2, and σ_3 given in Tables 1 and 2 are used. It was assumed in this analysis that the instantaneous values of the failure and strength differential effect tensors H_{ij} and h_i, as derived from the least square approximation scheme, belong to a certain failure surface of an equivalent orthotropic elastic body with values of H_{ij} and h_i those considered and this failure surface is progressively changing satisfying always the respective, experimentally obtained, values for the principal stresses.

However, one should notice that the calculated orthotropic elasticity coefficients are fictitious and they have generally nothing in common with the elasticity coefficients of the elastoplastic material. Moreover, they are not uniquely determined. Furthermore, the larger is the number of unknowns to be determined, the less accurate is the method. In order to check the stability and accuracy of the numerical procedure we have to define the limits of the constraint H_{bound} satisfying the inequality (10) or its respective bound concerning Eq. (19), which is expressed by:

$$G_{xx}\, G_{xy} - G_{xy}^2 \geq G_{bound} \tag{36}$$

This was necessary for studying the form and its variation inside the plastic zone of deformation of the failure hypersurface along its deviatoric plane, as well as its shape relatively to its axes of symmetry.

For purposes of high accuracy the limits of variation of H_{bound} and G_{bound} were taken between 1×10^{-11} and 1×10^{-9}. Furthermore, the numerical procedure of defining the failure hyperspace was based on different combinations of experimental data. The sets of hypersurfaces, derived from these combinations, created coherent entities of curves with insignificant deviations between them, thus indicating the stability of the method. Only when some of the initial values were selected at the borders of each loading zone, where either elacticity was in doubt, or the strain rates were rapidly changing, some scattering of these zones appeared in the plottings, which indicated the high sensitivity of the method. The satisfaction of the other constraints, that is either $H_{ij} > 0$, or $G_{ij} > 0$ did not present any difficulties.

The three distinctive steps of loading of the Naxian marble tested gave finally the following values of the terms of the respective tensors H_{ij} and h_i

contained in Table 1. The values of the terms of the respective tensors G_{ij} and g_i are readily given by relations (20). In the same table the values of the pairs of principal stresses in tension and compression σ_{Ti} and σ_{Ci} for the three loading steps are also tabulated. Having at our disposition these values of stresses and of the coefficients H_{ij} and h_i, we can readily define the various intersections of the failure hyperspaces.

a) The deviatoric plane of the EPFSs:

The center of this intersection, as well as the polar distance r_0 and the angle ψ_0, subtended by this polar distance and the 0''x''-axis of the paraboloid, are given by [14]:

$$x_0 = \sqrt{2}/3F \{2h_3(H_{11}-H_{22}) + h_1(3H_{33}-H_{11}+H_{22})-h_2(3H_{33}+H_{11}-H_{22})\}$$
$$y_0 = \sqrt{6}/9F \{h_1(5H_{22}-H_{33}-H_{11}) + h_2(5H_{11}-H_{22}-H_{33})-2h_3(2H_{11}+2H_{22}-H_{33})\} \quad (37)$$

with

$$F = \{2(H_{11}H_{22}+H_{22}H_{33}+H_{33}H_{11})-(H_{33}-H_{11})^2-(H_{11}-H_{22})^2-(H_{22}-H_{33})^2\}$$

$$\tan\psi_0 = \frac{\sqrt{3}}{3}\left\{\frac{h_1(5H_{22}-H_{33}-H_{11})+h_2(5H_{11}-H_{22}-H_{33})-2h_3(2H_{11}+2H_{22}+H_{33})}{2h_3(H_{11}-H_{22})+h_1(3H_{33}-H_{11}+H_{22})-h_2(3H_{33}+H_{11}+H_{22})}\right\} \quad (38)$$

Since the material is an orthotropic material, the orientation and the size of the intersection of the failure surface by the deviatoric plane, which is an ellipse, has its center outside the axis of symmetry of the paraboloid and its principal axes are subtending acute angles with the 0''x'' and 0''y''-axes of the surface.

Figure 5 presents the elliptic intersections of the failure hypersurface by the deviatoric π-plane and Table 1 the coordinates of the centers of the three ellipses corresponding to the three loading steps of the material. Furthermore, the polar distance r_0 and the inclination to the (-x)-axis of this radius, ψ_0, is given, as well as the lengths of the principal axes of the ellipses and their inclinations of the longest axis relatively to the (-x)-axis.

It is clear from this figure and the Table 1 that all centers of the ellipses lie inside the third compression-compression quadrant and their polar distances rotate antiblockwise while the anisotropy of the material is increasing as we advance inside the plastic zone of deformation.

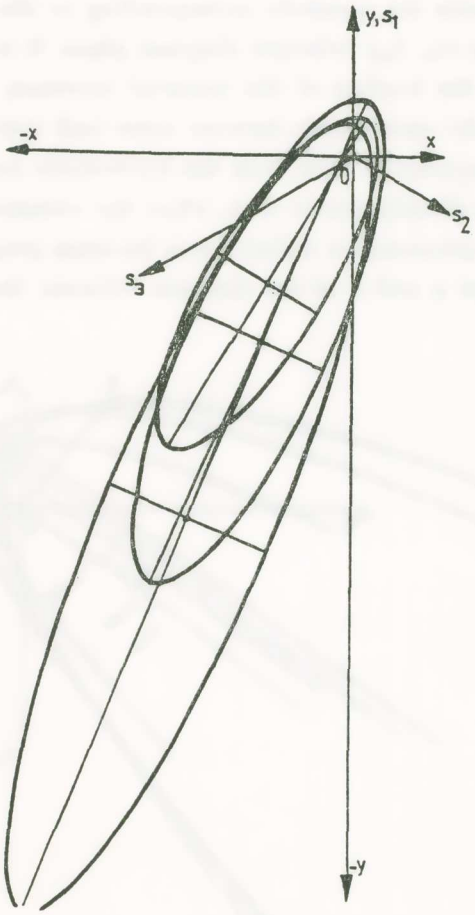

Fig. 5. Ta deviatoric plane intersectioàs of the EPFS for three ttypical loading steps of the Naxian marble.

b) The principal diagonal intersection of the elliptic paraboloid:

The intersections of the failure hyperspace by the three principal diagonal planes (σ_3,δ_{12}), (σ_1, δ_{23}) and (σ_2, δ_{13}) are all parabolas, whose axes of symmetry are parallel to the 0z-hydrostatic axis and lying at different distances from it, as the loading is progressing inside the plasticity zone. Their equations are derived from relation (17) by putting either $\delta_{21} = \sqrt{2}\ \sigma_1 = \sqrt{2}\ \sigma_3$ for the (σ_3, δ_{12})-plane, or $\delta_{23} = \sqrt{2}\ \sigma_2 = \sqrt{2}\ \sigma_3$ for the (σ_1, δ_{23})-plane, or $\delta_{13} = \sqrt{2}\ \sigma_1 = \sqrt{2}\ \sigma_3$ for the (σ_2, δ_{13})-plane. One of these equations for the (σ_3, δ_{12})-plane is given by relation (18).

Figure 6 presents the parabola corresponding to the intersection of the failure locus by the (σ_3, δ_{12})-principal diagonal plane. It is obvious from these plottings that, as the loading of the material increases, up to its ultimate strength, the elliptic paraboloids become more and more shallow, and the distances of their symmetry axes from the hydrostatic axis increase progressively. It has been already shown that, when the anisotropy of the material in increasing its representative failure locus becomes progressively shallower and the coordinates η and ξ of the distance between the symmetry axis of

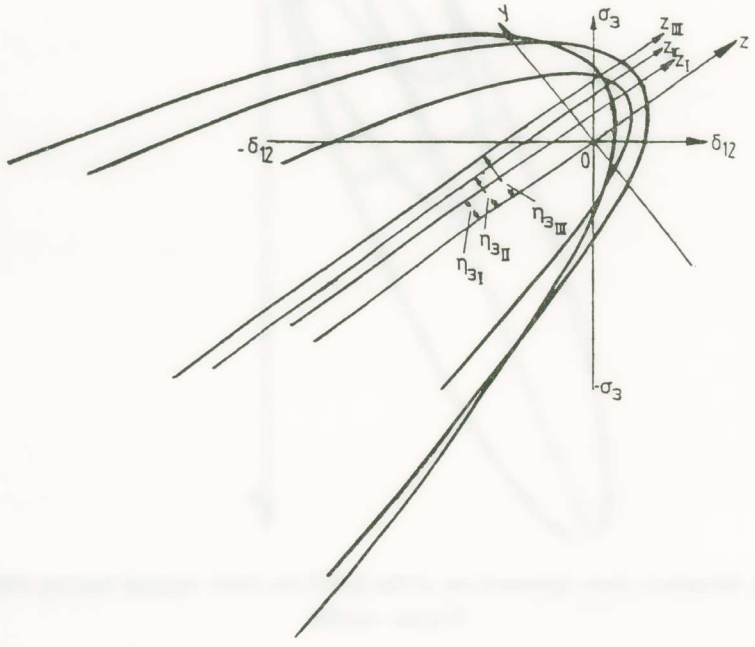

Fig. 6. The principal diagonal plane (σ_3, δ_{12})-intersections of the EPFS for three typica loading steps of the Naxian marble.

the paraboloid and the hydrostatic axis are also increasing. These distances for the orthotropic material are given by complicated relationships for the general orthotropic material and they are not given here. These relationships for the transversely isotropic material are considerably simplified and they are given in Ref. [14].

Table 1 gives the characteristic dimensions of the principal diagonal (σ_3, δ_{12})-plane, that is its equation with the coefficients α, β, γ, the coordinates

of the vertex of the (σ_3, δ_{12})-parabola, as well as the distances η_i and ξ_i between its symmetry axis and the hydrostatic axis along the y- and x-axes of the EPFS.

Then, the EPFSs for the general orthotropic material have their axes of symmetry parallely displaced, relatively to the hydrostatic axis, but moving outside the principal diagonal planes. Indeed, for the orthotropic materials the respective EPFSs are angularly displaced, so that the centers of their transverse elliptic intersection lie outside the principal diagonal planes and their planes of symmetry O''y''z'' or O''x''z'' are intersecting the principal diagonal planes along lines parallel to the hydrostatic axis, whose traces on the deviatoric plane are points S (for the O''y''z''-plane) different than the origin O.

c) The principal (σ_i, σ_j)-stress intersections of EPFS.

The equations expressing the intersections of the failure hypersurface by the principal stress planes are given as follows: For the (σ_1, σ_3)-principal plane the following equation in this plane expresses this principal intersection. This comes out from relation (16) by putting $\sigma_2 = 0$. It is valid that:

$$H_{11}\sigma_1^2 + H_{33}\sigma_3^2 + 2H_{31}\sigma_3\sigma_1 + h_1\sigma_1 + h_3\sigma_3 = 1 \tag{39}$$

The center of this ellipse is defined by its coordinates $(\sigma_{3M}, \sigma_{1M})$. Figure 7 presents this intersection in the (σ_3, σ_1)-principal stress plane and the coordinates σ_{3M}, σ_{1M} and the angle λ_1 of inclination of the polar radius (OM) are given by [14]:

$$(\sigma_{3M}, \sigma_{1M}) = \left\{ \frac{\frac{1}{2}(h_3H_{31}-h_1H_{33})}{(H_{11}H_{33}-H_{31}^2)}, \frac{\frac{1}{2}(h_1H_{31}-h_3H_{11})}{(H_{11}H_{33}-H_{31}^2)} \right\} \tag{40}$$

$$\lambda_1 = \tan^{-1}(h_1H_{33}-h_3H_{11})/h_3H_{33} \tag{41}$$

The system of Cartesian coordinates (M- σ_1, σ_3), to which this ellipse is central and symmetric, is defined by the angle θ_1, expressed by:

$$\theta_1 = 1/2\tan^{-1}[2H_{31}/(H_{33}-H_{11})] \tag{42}$$

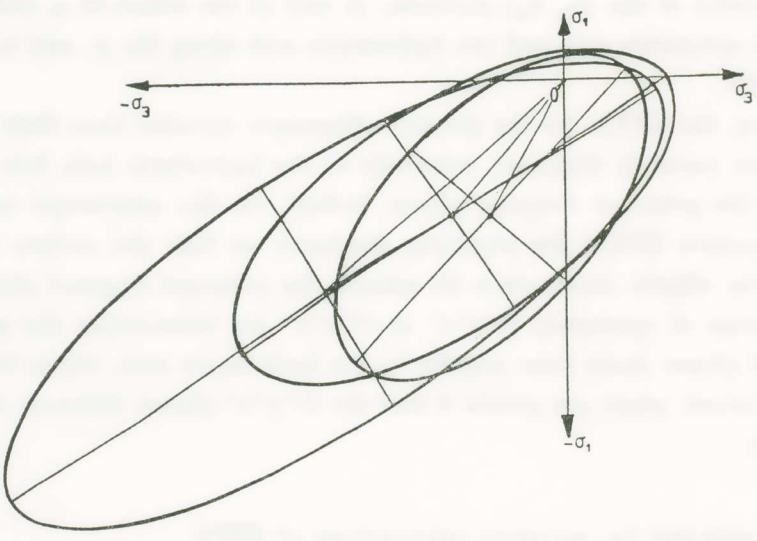

Fig. 7. The (σ_1, σ_3)-principal stress plane intersections of the EPFS for three typical loading steps of the Naxian marble.

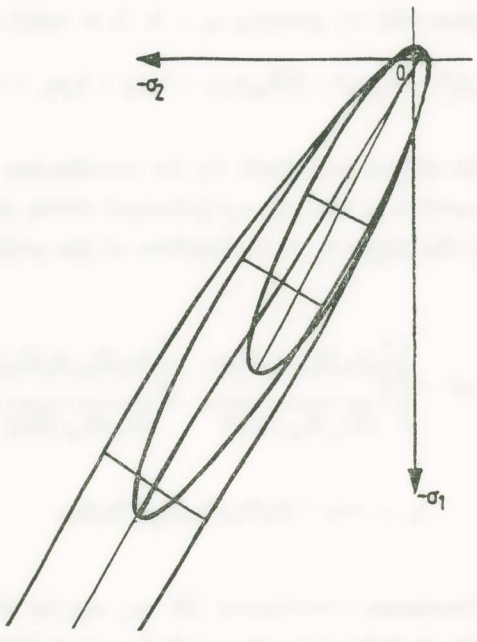

Fig. 8. The (σ_1, σ_2)-principal stress plane intersections of the EPFS for three typical loading steps of the Naxiap marble.

whereas the semi-axes a_{1M} and a_{3M} of the ellipse are given by [14]:

$$a_{1M} = \left(\frac{1}{\bar{a}}\right)^{1/2}\left\{1 + \frac{H_{11}h_3^2 + H_{33}h_1^2 - 2h_1h_3H_{31}}{(H_{11}-H_{22})^2 + H_{33}(4H_{12}-H_{33})}\right\}^{1/2} \tag{43}$$

$$a_{3M} = \left(\frac{1}{\bar{b}}\right)^{1/2}\left\{1 + \frac{H_{11}h_3^2 + H_{33}h_1^2 - 2h_1h_3H_{31}}{(H_{11}-H_{22})^2 + H_{33}(4H_{12}-H_{33})}\right\}^{1/2} \tag{44}$$

and

$$\begin{aligned} \bar{a} &= \frac{1}{2}\left\{(H_{11} + H_{33}) + \left[(H_{33}-H_{11}^2) + 4H_{31}^2\right]^{1/2}\right\} \\ \bar{b} &= \frac{1}{2}\left\{(H_{11} + H_{33}) - \left[(H_{33}-H_{11}^2) + 4H_{31}^2\right]^{1/2}\right\} \end{aligned} \tag{45}$$

Similar relationships are valid for the two other principal stress planes ((σ_1, σ_2) and (σ_2, σ_3)), where these equations are established by cyclid rotation of the indices.

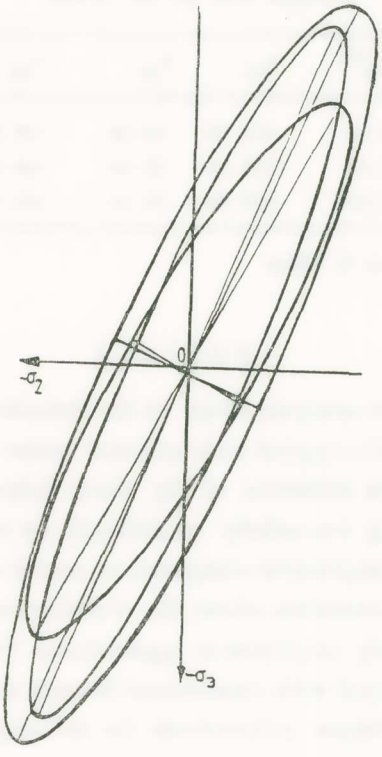

Fig. 9. The (σ_2, σ_3)-principal stress plane intersections of the EPFS for three typical loading steps of the Naxian marble.

Table 2 contains all the necessary dimensions for plotting these intersections. Thus, the σ_{iM}, σ_{jM} coordinates of the centers of the ellipses, as well as their polar distances for the origin O are given, complemented by the polar angles λ_{ij}, of these polar distances. Similarly, the principal semi-axes of the ellipses are given together with the orientation of their major axes, relatively to the principal frames of the EPFS. Furthermore, Figs. 7 to 9 present these intersections for the Naxian marble tested.

From all these values of the coefficients of the terms of the failure tensor polynomials the values of the principal stresses in simple tension and compression along the principal directions of the materials are readily evaluated using relations (11) and (12) and they are given in Table 3.

TABLE 3

The values of the principal stresses in tension (σ_{Ti}) and compression (σ_{Ci}) along the three principal axes for the EPFSs

Loading Steps	$\sigma_{T1}^{(*)}$	σ_{C1}	σ_{T2}	σ_{C2}	σ_{T3}	σ_{C3}
Elastic (I)	24.54	-210.60	39.49	-39.69	68.20	-69.11
Initial Yielding (II)	30.39	-193.88	48.30	-48.56	101.55	-103.16
Ultimate Strength (III)	15.10	-193.36	34.11	-34.78	79.12	-80.02

All components of stresses in MPas.

7. RESULTS

From the extensive analysis, based on the definition of failure surfaces in various loading steps of a typical rock material under elastic and plastic modes of deformation, the evolution of the whole failure hypersurface of this material during loading was solidly established, by using only uniaxial and triaxial compression-compression-compression modes of loading, yielding reliable and complete information about the evolution of strength of the material, which can be readily employed in applications. The least square numerical analysis was employed with constrained bounds derived from the respective theory of failure tensor polynomials for defining yield loci of the materials.

The method succeeds to solve completely the problem of the definition of

the failure loci of a material deformed progressively in the elastic and plastic, up to its ultimate strength, by using only experimental data concentrated in a small area of the yielding, conveniently selected to give reliable and accurate experimental data. In this paper three characteristic steps of loading of a granular rock were considered, that is in its elastic range, in the initial yielding defined by a conventional strain of 0.02% and finally at its ultimate strength. The experimental data were all concentrated in the compression-compression-compression octant of the yield locus, where these tests could be effectively executed. The method succeds to yield a full picture of the failure hypersurface of the material, based on data belonging in the underbelly of the yield locus.

Provided that the problem considered is of the type of proportionate loading, for which the classical flow theory of plasticity is valid, it is possible to proceed to interpolations in-between the basic loading steps, for which experimental tests are executed, and define the details of the variations of the mechanical properties of the material, as the loading proceeds inside the plastic zone.

This procedure is more accurately established by using, instead of the least square numerical method developed here, a method of parameter identification, realized in an appropriate neural network environment, through supervised and unsupervised learning algorithms. This method, which is introduced and extensively developed in refs. [19] and [20], presents certain definite advantages over the classical numerical analysis with adjoining constraints, derived from applying optimization problems, based on neural network approach, where the anisotropic hardening elastoplastic behaviour is approximated by a fictitious convenient material, whose properties are adapted to the existing experimental data. This method will be the subject of a companion paper.

Figures 5 to 9 present the intersections of the elliptic paraboloid failure hypersurface by different characteristic planes. It is clear from these figures that the material is strongly anisotropic with variable anisotropy, if the material is loaded inside the plastic zone. Moreover, the compression strength of the material is very pronounced and increasing as the loading is progressing.

However, it is of interest to study separately the influence of anisotropy of the material per se, and the influence of the strength differential effect. Table 3 indicates the values of the yielding stresses in triaxial loading, as the

loading is progressing. Examining the values of the terms h_i, responsible exclucively for the strength differential effect, one observes the striking difference between the values of h_1 and, on the other hand, the respective values of h_2 and h_3. These values are a hundred time smaller than h_1 and almost equal. This phenomenon indicates that the strength differential effect at the plane (σ_2, σ_3) of symmetry, is insignificant. Figure 9 indicates the same phenomenon. The three elliptic intersections by the (σ_2, σ_3)-plane of the EPFSs at different steps of loading have their centers almost at the origin O of the coordinate system $\sigma_2 O \sigma_3$, thus resulting to almost equal tension and compression stresses along the principal axes of the ellipses.

This phenomenon may be explained by the form of structure of this type of marble. Indeed, Naxian marble is belonging to the **cataclastic family** of rocks derived from igneous parent rocks. These rocks are produced by a dynamic metamorphism during which, faulting, granulation and flowage may occur in previously crystalline parent rocks, because of stresses exceeding their breaking strength. Then, the individual minerals in the rock may selectively granulated. Movements in preferred directions may occur with slippage planes and granulation being oriented preferentially. Thus, partially destroyed rocks create streaks swirling around still undestroyed rock. It is accepted that Naxian marbles are products of extreme cataclastic deformation. They are fine grained and laminated, creating closely spaced slippage surfaces giving to the rock a fissility. Figure 10 shows a cross-sectional view of a phyllite type rock, indicating intense stretching spots, forming parallel laminae similar to those typically existing in the Naxian marbles.

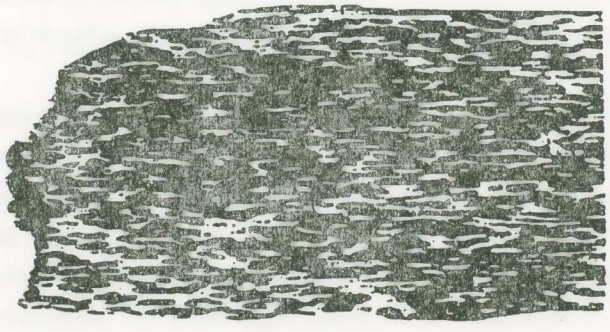

Fig. 10. Cross sectional view of a spotted phyllite rock showing spots of chlorite in a staggered arrangement.

On the other hand, foamy materials and other modern composites with a weak reinforcing phase, arranged in a zig-zag distribution of their oblong inclusions, belong to a special category of materials presenting very low values and in some staggering arrangements, negative values of their Poisson's ratios along the transverse planes of laminae. An analytic study of such composites, whose configuration resembles the arrangement of Fig. 10, gave Poisson's ratios of the order of -O.20 to O.60, for the plane normal to the plane of laminae [24]. Values of Poisson's ratios for Naxian and Parian marbles have been accurately measured and found to be $\nu_n = 0.08$ for the Naxian marble and $\nu_p = 0.80$ for the Parian marble along the normal plane to the laminae [25]. This coincidence of results constitutes another proof of the correctness of the results derived from application of the theory of failure tensor polynomials with variable terms inside the plastic zones of deformation.

REFERENCES

[1] A. A. Ilyushin, On the Increment of Plastic Deformation and Yield Function, Prikl. Math. Mech. 24 (1960) 663-666.

[2] A. E. Green and P. M. Naghdi, A General Theory of an Elastic-Plastic Continuum, Arch. Rat. Mech. Anal. 18 (1965) 251-281.

[3] A. Zhukov, Plastic Deformation of Isotropic Metals in Combined Loading, Izw. Akad. Nauk. SSSR. OTN 12 (1956) 72-87.

[4] K. Ikegami, A Historical Perspective of the Experimental Study of Subsequent Yield Surfaces for Metals Part I, J. Soc. Mat. Sci. 24 (1975) 491-505.

[5] K. Ikegami, An Historical Perspective of the Experimental Study of Subsequent Yield Surfaces for Metals Part II, J. Soc. Mat. Sci. 24 (1975) 709-719.

[6] H. Ziegler, A Modification of Prager's Hardening Rule, Quart. Appl. Math. 14 (1959) 55-65.

[7] E. Shiratori and K. Ikegami, Experimental Study of the Subsequent Yield Surface by using Cross-shaped Specimens, Jnl. Mech. Phys. Solids 16 (1968), 373-394.

[8] E. Shiratori, K. Ikegami, and K. Kaneko, Subsequent Yield Surfaces Determined in Consideration of the Bauschinger Effect in Foundations of Plasticity (ed. by A. Sawczuk) Noordhoff Int. Publ., Leyden, 1973.

[9] E. Shiratori, K. Ikegami, and F. Yoshida, Analysis of Stress-Strain Relation by use of an Anisotropic Hardening Plastic Potential, Jnl. Mech. Phys. Solids 27 (1979) 213-229.

[10] D. W. A. Rees, A multi-surface representation of anisotropic hardening and comparisons with experiment, Proc. Inst. Mech. Engrs. 198C (1984) 269-282.

[11] M. Ortiz and E. P. Popov, Distortional Hardening Rules for Metal Plasticity ASCE, EM, 109 (1983) 1042-1057.

[12] Z. Mroz, On the Description of Anisotropic Work-Hardening, Jnl. Mech. Phys. of Solids, 15 (1967) 163-175.

[13] Y. F. Dafalias and E. P. Popov, A Model of Non-linearly Hardening Material for Complex Loading, Acta Mechanica, 21 (1975) 173-192.

[14] P. S. Theocaris, Failure Criteria for Anisotropic Bodies, Handbook of Fatigue Crack Propagation in Metallic Structures, A. Carpinteri Editor, Elsevier, Amsterdam, Publ., 1, (1994) 3-45.

[15] P. S. Theocaris, Failure Criteria for Engineering Materials Based on Anisotropic Hardening, Proc. Nat. Acad. Athens, Ser. A61 (1986) 84-114.

[16] P. S. Theocaris, Failure Characterization of Anisotropic Materials by Means of the Elliptic Paraboloid Failure Criterion, Uspechi Mechaniki (Advances in Mechanics) 10 (1987) 83-102.

[17] P. S. Theocaris, The Elliptic Paraboloid Failure Surface for Transversely Isotropic Materials off-axis Loaded, Rheologica Acta, 28 (1989) 154-165.

[18] P. S. Theocaris, The Paraboloid Failure Surface for the general orthotropic material, Acta Mechanica, 79(1), (1989) 53-79.

[19] P. S. Theocaris and P. D. Panagiotopoulos, Plasticity Including the Bauschinger effect Studied by a Neural Network Approach, Acta Mechanica, 113, 1-4, (1995) pp. 63-75.

[20] P. S. Theocaris and P. D. Panagiotopoulos, Generalized Hardening Plasticity Approximated via Anisotropic Elasticity: A Neural Network Approach, Computer Methods in Appl. Mech. and Engng., 125 (No 1) (1995), 123-139.

[21] P. N. Michelis, Work softening and hardening behaviour of granular rocks, Rock Mechanics, 14 (1981) 187-200.

[22] A. J. MacConnell, Applications of Tensor Analysis, Dover Publ. Inc. New York 1957.

[23] F. D. Murnaghan, Analytic Geometry, Prentice Hall Inc. N. York (1946).

[24] P. N. Michelis, Polyaxial yielding of granular rock, Jnl. Engng. Mechanics, Proc. ASCE, 111 (8), (1985) 1049-1066.

[25] P. S. Theocaris, The Mechanics of Cellular Materials with Negative Poisson's ratios, Intern. Jnl. of Damage Mechanics, submitted for publication (1995).

ΠΕΡΙΛΗΨΙΣ

ΓΕΝΙΚΗ ΜΕΘΟΔΟΣ ΠΡΟΣΔΙΟΡΙΣΜΟΥ ΤΩΝ ΝΟΜΩΝ ΠΛΑΣΤΙΚΟΤΗΤΟΣ ΑΝΙΣΟΤΡΟΠΩΝ ΥΛΙΚΩΝ

Εἰς τὴν ἀνακοίνωσιν αὐτὴν εἰσάγεται μέθοδος προσδιορισμοῦ διαδοχῆς νόμων, ὑπακουόντων τμηματικῶς εἰς τὰς ἀρχὰς τῆς γραμμικῆς ἐλαστικότητος, κατὰ τὴν ὁποίαν σῶμα τῆς αὐτῆς γεωμετρίας καὶ τῆς αὐτῆς διαδοχῆς φορτίσεων καὶ τῶν αὐτῶν περιορισμῶν, παρουσιάζει συμπεριφορὰν ταυτόσημον μὲ τὴν συμπεριφορὰν τοῦ ὑπὸ ἐξέτασιν ἐλαστο-πλαστικοῦ ἀνισοτρόπου σώματος.

Ἐὰν p (t) ἐκφράζει τὴν συνάρτησιν φορτίσεως ἐντὸς τοῦ διαστήματος $t \in [0, T]$, τὸ διάστημα αὐτὸ διαιρεῖται εἰς τὰ ὑποδιαστήματα $[0, T] \to t^{(1)}, t^{(2)}, t^{(3)} \ldots, t^{(n)}$ κατὰ τὰ ὁποῖα ἰσχύουν ἀντιστοίχως οἱ ἐπὶ μέρους ἀνισότροποι ἐλαστικοὶ τανυσταί: $C^{(1)}, C^{(2)}, C^{(3)} \ldots, C^{(n)}$

Ζητοῦμεν τὴν σχέσιν $\{t^{(\rho)}, C^{(\rho)}\}$, $\rho = 1, 2, 3, \ldots, n$, τοιαύτην ὥστε ἡ λύσις τοῦ ἀνισοτρόπου προβλήματος ἐλαστικότητος νὰ προσεγγίζει κατὰ τὸ δυνατὸν πλησιέστερον τὴν λύσιν τοῦ ζητουμένου ἐλαστο-πλαστικοῦ προβλήματος.

Τὸ πρόβλημα διαμορφώνεται ὡς πρόβλημα **παραμετρικῆς ταυτοποιήσεως**, ὅπου $z^{(\rho)} = \{t^{(\rho)}, C^{(\rho)}\}$ εἶναι αἱ ἐλέγχουσαι παράμετροι καὶ αἱ συνιστῶσαι τῶν τάσεων $\sigma^{(\rho)}$, παραμορφώσεων $\varepsilon^{(\rho)}$, καὶ μετατοπίσεων $u^{(\rho)}$ ἐκφράζουν τὰς καταστατικὰς συναρτήσεις, αἱ ὁποῖαι δίδονται ἀπὸ τὸ πρόβλημα διὰ τῶν ἐπὶ μέρους πειραμάτων.

Δεχόμενοι βήματα μικρῶν μετατοπίσεων καὶ παραμορφώσεων, ὁρίζομεν τὰς διαφοράς:

$$A_1 = \sum_{\rho=1}^{n} \int_{\Omega} \left[u_{pl}^{(\rho)} - u_{el_n}^{(\rho)} \right]^2 d\Omega,\ A_2 = \sum_{\rho=1}^{n} \int_{\Omega} \left[\varepsilon_{pl}^{(\rho)} - \varepsilon_{el}^{(\rho)} \right]^2 d\Omega,\ A_3 = \sum_{\rho=1}^{n} \int_{\Omega} \left[\sigma_{pl}^{(\rho)} - \sigma_{el}^{(\rho)} \right]^2 d\Omega \quad (1)$$

Τὸ πρόβλημα τίθεται νὰ ὁρισθῇ ἡ σχέσις $z^{(\rho)}{}_\iota = \{t^{(\rho)}, C^{(\rho)}\}$, $\rho = 1, 2, 3, \ldots, n$, οὕτως ὥστε νὰ ἱκανοποιῇ, δι' οἱανδήποτε τιμὴν τοῦ ρ, τὴν συνθήκην:

$$A_1 + A_2 + A_3 \to \min \quad (2)$$

ὅπου τὰ μεγέθη $\sigma_{el}^{(\rho)}$, $\varepsilon_{el}^{(\rho)}$ καὶ $u_{el}^{(\rho)}$ πρέπει νὰ ἱκανοποιοῦν τὰς ἐξισώσεις ἰσορροπίας τοῦ συστήματος καὶ τὰς σχέσεις τάσεων-παραμορφώσεων, ἐνῶ τὰ ἀντίστοιχα πλαστικὰ μεγέθη πρέπει ἐπὶ πλέον νὰ ἱκανοποιοῦν τὰς ἀντιστοίχους πειραματικὰς τιμὰς καὶ τὰς σχέσεις πλαστικότητος.

Ἐλαχιστοποιῶντας τὴν συνθήκην (2) λαμβάνομεν:

$$P \sum_{\rho=1}^{n} \left[\sum_{r=1}^{m} \left(\left\| \varepsilon_{pl}^{(\rho)(r)} - \varepsilon_{el}^{(\rho)(r)} (z^{(\rho)}) \right\|^2 + \left\| \sigma_{pl}^{(\rho))r)} - \sigma_{el}^{(\rho)(r)} (z^{(\rho)}) \right\|^2 \right) \right] \to \min \quad (3)$$

$$K(z^{(\rho)}\, u^{(\rho)}) + p^{(\rho)} = 0 \qquad (4)$$

ὅπου $\rho^{(9)}$ παριστᾶ τὴν συνάρτησιν φορτίσεως διὰ τὸ βῆμα φορτίσεως ρ.

Ἡ σχέσις (3) γράφεται καὶ ὡς ἀνισότης ὡς ἑξῆς:

$$\max_{p,r,i,j} \left| \varepsilon^{(\rho)(r)}_{plij} - \varepsilon^{(\rho)(r)}_{elij} (z^{(\rho)}) \right| \leqslant \delta, \ \max_{p,r,i,j} \left| \sigma^{(\rho()r)}_{plij} - \sigma^{(\rho)(r)}_{elij} (z^{(\rho)}) \right| \leqslant \delta, \qquad (5)$$

ὅπου δ παριστᾶ τὸν ἐπιβαλλόμενον σύνδεσμον.

Διὰ τὸν καθορισμὸν τῶν συνιστωσῶν τῶν τάσεων διαρροῆς εἰς τὸ ὑπὸ ἐξέτασιν βῆμα φορτίσεως χρησιμοποιοῦμεν τὰς συνθήκας γενικῆς διαρροῆς ἀνισοτρόπων ὑλικῶν, ἐκπεφρασμένας μὲ τανυστικὰ πολυώνυμα ἀστοχίας, καὶ δὴ μὲ τὸ **ἐλλειπτικὸν παραβολοειδὲς κριτήριον διαρροῆς**, αἱ ὁποῖαι ὑπολογίζονται ὑπὸ κλειστὴν μορφήν, γνωστῶν οὐσῶν τῶν κυρίων τάσεων εἰς ἐφελκυσμὸν καὶ θλῖψιν τοῦ σώματος κατὰ τὰς τρεῖς κυρίας διευθύνσεις τῆς βαθμίδος φορτίσεως.

Ἡ ὡς ἄνω θεωρία ἐφηρμόσθη ἐπὶ δεδομένων διαρροῆς καὶ ἀστοχίας **Παρίου μαρμάρου**, καταπονουμένου εἰς διαφόρους συνδυασμοὺς τριαξονικῆς θλίψεως. Ἐκ τῶν δεδομένων εἰς τὴν περιορισμένην περιοχὴν φορτίσεως θλίψεως κατὰ τοὺς τρεῖς ἄξονας ὑπελογίσθη πλήρως καὶ μὲ μεγάλην ἀκρίβειαν ὁ νόμος ἀστοχίας τοῦ ὑλικοῦ διὰ διαφόρους τύπους φορτίσεως καὶ προέκυψαν σημαντικοὶ νόμοι παραμορφώσεως τῶν ὑλικῶν εἰς τὴν πλαστικὴν περιοχὴν γιὰ τὴν γενικωτάτην περίπτωσιν τοῦ ἀνισοτρόπου ἐλαστο-πλαστικοῦ ὑλικοῦ, παρουσιάζοντος καὶ φαινόμενα διαφορικῆς ἀντοχῆς.